Chemical Physics Publications   Department of Chemical Physics

7-20-2006

Electric Heating Effects in Nematic Liquid Crystals

Y. Yin
Kent State University - Kent Campus

Sergij V. Shiyanovskii
Kent State University - Kent Campus

Oleg Lavrentovich
Kent State University - Kent Campus, olavrent@kent.edu

Recommended Citation

Yin, Y.; Shiyanovskii, Sergij V.; and Lavrentovich, Oleg (2006). Electric Heating Effects in Nematic Liquid Crystals. *Journal of Applied Physics* 100(2). doi: 10.1063/1.2214466 Retrieved from http://digitalcommons.kent.edu/cpippubs/190

Electric heating effects in nematic liquid crystals

Y. Yin, S. V. Shiyanovskii, and O. D. Lavrentovich[a)]

Chemical Physics Interdisciplinary Program, Liquid Crystal Institute, Kent State University, Kent, Ohio 44242

Electric heating effects in the nematic liquid crystal change the liquid crystal physical properties and dynamics. We propose a model to quantitatively describe the heating effects caused by dielectric dispersion and ionic conductivity in the nematic liquid crystals upon the application of an ac electric field. The temperature increase of the liquid crystal cell is related to the properties of the liquid crystal such as the imaginary part of the dielectric permittivity, thermal properties of the bounding plates, and the surrounding medium as well as frequency and amplitude of the electric field. To study the temperature dynamics experimentally, we use a small thermocouple inserted directly into the nematic bulk; we assure that the thermocouple does not alter the thermal behavior of the system by comparing the results to those obtained by a noncontact birefringent probing technique recently proposed by Wen and Wu [Appl. Phys. Lett. **86**, 231104 (2005)]. We determine how the temperature dynamics and the stationary value of the temperature increase depend on the parameters of the materials and the applied field. We used different surrounding media, from extremely good heat conductors such as aluminum cooling device to extremely poor conductor, Styrofoam; these two provide two limiting cases as compared to typical conditions of nematic cell exploitation in a laboratory or in commercial devices. The experiments confirm the theoretical predictions, namely, that the temperature rise is controlled not only by the heat transfer coefficient of the surrounding medium (as in the previous model) but also by the thickness and the thermal conductivity coefficient of the bounding plates enclosing the nematic layer. The temperature increase strongly depends on the director orientation and can change nonmonotonously with the frequency of the applied field. © *2006 American Institute of Physics*. [DOI: 10.1063/1.2214466]

I. INTRODUCTION

Dielectric properties of liquid crystals (LCs) depend on the frequency of the applied field, as the dipolar groups of LC molecules experience complex motion strongly influenced by the orienting neighborhood.[1] There are few characteristic times associated with various modes. Usually, rotation of the longitudinal dipole component around the short molecular axis gives rise to the dielectric relaxation with the lowest frequency that is detected in the frequency dependency of the parallel component of dielectric permittivity $\varepsilon_\parallel(f)$.[2,3] Orientational order of LC molecules shifts the dispersion region of $\varepsilon_\parallel(f)$ to the frequencies lower than those for the isotropic phase. At higher frequencies, the relaxation phenomena are associated with other types of motions, such as rotation of the longitudinal dipole component around the director **n** that contributes to the frequency dependence of the perpendicular component $\varepsilon_\perp(f)$ and rotation of the perpendicular dipole component around the long molecular axis that contributes to both $\varepsilon_\parallel(f)$ and $\varepsilon_\perp(f)$. There are two important general consequences of the dielectric relaxation phenomena: (1) nonlocal time relationship between the electric displacement and the electric field and (2) dielectric heating. The first effect is simply a reflection of the fact that the electric displacement, being the function of both the applied field and the material's properties, needs some finite time to adjust to the value of the electric field. The second effect is

related to the efficiency of absorption of electromagnetic energy by the dielectric medium through reorientation of the molecular dipoles and the associated molecular friction.[2–5] This absorption is small when the frequency of the applied field is too high or too low as compared to the relaxation frequency, but it becomes very efficient in the region of dielectric relaxation. Although the two effects are common for all types of dielectrics, they acquire especially interesting facets for the case of a liquid crystal dielectric. Both effects can greatly influence the performance of devices such as LC displays, especially when the effective frequency characterizing the change of the applied electric field approaches the region of dielectric relaxation; in this case, the rotating torque acting on the LC becomes a function of not only the instantaneous values of the electric field and the orientation of the director, but also of the past values of these variables.[6]

The study of the phenomenon of dielectric heating of a nematic LC (NLC) has been performed by Schadt.[7] In his model, the temperature decrease across the bounding (glass) plates of the NLC cell was considered negligibly small. The temperature rise caused by dielectric heating was measured for NLC cells with a thickness of 15 μm by a thermocouple with an 80 μm head (placed apparently outside the NLC bulk).[7] The corresponding model assumed that there is no temperature gradients across the bounding glass plates of the cell (regardless of the medium in which the entire NLC cell is located). As we shall see later, the temperature gradients across the glass substrates of the cell can be substantial and reach several degrees. These studies[7] were expanded in our

a)Electronic mail: odl@lci.kent.edu

previous work by using a much smaller thermocouple inserted directly into the NLC slab.[8] Recently, Wen and Wu proposed a noncontact method[9] based on the measurements of phase retardation changes caused by the temperature-induced changes of the birefringence Δn of the NLC. This technique is applicable when the electric field causes no reorientation of the director (otherwise the phase retardation would change because of the director reorientation), i.e., when the following conditions are satisfied: (1) the material has a negative dielectric anisotropy, $\varepsilon_\parallel(f) - \varepsilon_\perp(f) \leqslant 0$, (2) the cell yields a strict planar alignment (zero pretilt angle), and (3) the electric field causes no hydrodynamics. Because of these limitations, the technique cannot address the issue of dielectric heating in the region of dielectric relaxation for $\varepsilon_\parallel(f)$. The previous work, therefore, does not provide a complete picture of electric heating effects in a nematic sample, especially the role of bounding plates and director orientation.

In this work, we explore the electric heating effects of NLC cells in an ac electric field caused by the dielectric relaxation and by the ionic currents of the NLC (although the latter can be neglected at field frequencies higher than a few kilohertz). To measure the temperature of the nematic slab in the broad range of field frequencies directly, we use a tiny thermocouple (head size of 25 μm) inserted into the 40 μm thick NLC slab. We verify that the presence of thermocouple does not affect the thermal behavior of the sample by comparing the data to data obtained with the noncontact birefringence technique[9] for the case when all the three conditions [(1)–(3)] above are satisfied. We perform experimental studies for a variety of surrounding media with different heat transfer properties and for different frequencies of the applied field, including those that correspond to different regions of dielectric relaxation. We propose a theoretical model that incorporates the finite thermal conductivity of the bounding plates. The experiments confirm the theoretical predictions, such as that the temperature rise is controlled not only by the heat transfer coefficient of the surrounding medium but also by the thickness and the thermal conductivity coefficient of the bounding plates and director orientation.

We first address the theoretical model and then compare it to the experimental data.

II. THEORY

When a nematic cell is driven by a harmonic electric field $\mathbf{E} = \mathbf{E}_0 \cos 2\pi f t$, the heating power density P caused by the dielectric relaxation and the ionic current in NLC can be written as[1]

$$P = f \int_0^{1/f} \mathbf{E}\left(\frac{\partial \mathbf{D}}{\partial t} + \mathbf{J}\right) dt = \pi f \varepsilon_0 \mathbf{E}_0 \cdot \varepsilon^i \cdot \mathbf{E}_0 + \frac{1}{2}\mathbf{E}_0 \cdot \sigma \cdot \mathbf{E}_0,$$

(1)

where $\mathbf{D}$ is the electric displacement, $\mathbf{J}$ is the current density, ε^i is the imaginary part of the dielectric tensor ε of the NLC, and σ is the conductivity tensor of the NLC. The tensors ε and σ and thus the heating power density P depend on the orientation of the NLC director $\mathbf{n}$. In what follows, for the sake of simplicity, we assume that the electric field is homo-

geneous inside the cell. This assumption is valid under two conditions. First, the frequency f should be high enough to make the ionic screening of the applied field negligible; usually, it means $f > 1$ kHz.[2,10] Second, the director field should be uniform or only weakly distorted across the cell (including the case of a very strong voltage when most of the NLC is reoriented) or the dielectric and conductivity anisotropies of the LC material should be weak. If these conditions apply, we can represent the electric field through the applied voltage U acting across a NLC cell of a thickness d, $\mathbf{E}_0 = U\hat{\mathbf{z}}/d$, so that

$$P = \frac{\pi f \varepsilon_0 \varepsilon_{zz}^i U^2}{d^2} + \frac{\sigma_{zz} U^2}{2d^2},$$

(2)

where $\varepsilon_{zz}^i = \varepsilon_\perp^i \sin^2 \theta + \varepsilon_\parallel^i \cos^2 \theta$ is the imaginary part of the effective dielectric permittivity, $\sigma_{zz} = \sigma_\parallel \sin^2 \theta + \sigma_\perp \cos^2 \theta$ is the effective ionic conductivity of the material, and θ is the angle between the director $\mathbf{n}$ and the normal $\hat{\mathbf{z}}$ of the bounding plates.

Let us discuss now the scheme of the electrically induced heat production and its transfer in the multilayered system comprised of a NLC layer, two bounding plates of finite thickness (but of infinite size in the two other directions), placed into some surrounding medium of infinite extension, Fig. 1.

The heat conduction equation for each of the layers is of a generic form[11]

$$c_p \rho \frac{\partial T(z,t)}{\partial t} = G \frac{\partial^2 T(z,t)}{\partial z^2} + P_0,$$

(3)

where c_p is the heat capacity of the layer, ρ is the material density, G is the layer's thermal conductivity, and P_0 is the specific heat production inside the layer. Equation (3) should be accompanied with the boundary conditions that guarantee the heat flow balance.

For the case of the NLC layer, $P_0 = P$. The temperature drop across the NLC slab $\Delta T_{\text{LC}}(t)$ reaches its maximum for a stationary regime. Equation (3) allows us to determine it as $\Delta T_{\text{LC}}(t) \leqslant Pd^2/8G_{\text{LC}} = (2\pi f \varepsilon_0 \varepsilon_{zz}^i + \sigma_{zz})U^2/16G_{\text{LC}}$, where G_{LC} is the thermal conductivity of the liquid crystal. For a typical situation, $G_{\text{LC}} \approx 0.2$ W m^{-1} K^{-1},[12] $\varepsilon_{zz}^i \approx 1$, $U \leqslant 50$ V, $f \leqslant 10^6$ Hz, and $\sigma_{zz} \approx 10^{-9}$ Ω^{-1} m^{-1}, the temperature drop is less than about 0.05 °C. Therefore, we can assume that the temperature drop across the (relatively thin) NLC layer is small and concentrate on the temperature changes in the bounding plates.

In what follows, we consider the system being symmetric with respect to the middle plane of the NLC cell and apply Eq. (3) to describe the heat conduction through one of the two bounding plates, for example, the one located within $z \in [d/2, d/2 + L]$ or $\tilde{z} \in [0, L]$, where $\tilde{z} = z - d/2$ is introduced to simplify the notations. Equation (3) needs to be supplemented by two boundary conditions for the heat transfer, at the NLC-bounding plate interface and at the bounding plate-surrounding medium interface. Because the NLC layer is thin as compared to the bounding plates, one can neglect the heat stored in the NLC layer itself, so that the heat flux from the NLC layer to the bounding plate is $Q_{\text{in}} = Pd/2$. We as-
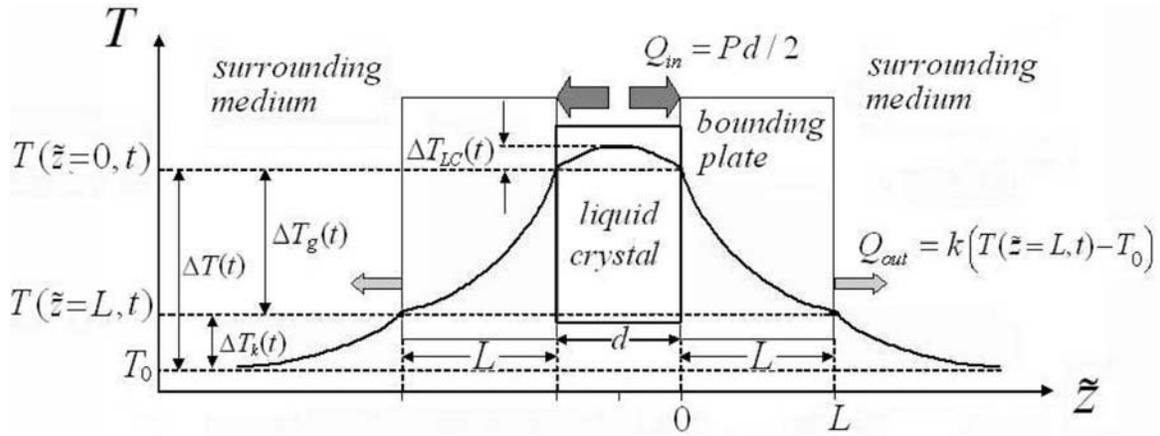
FIG. 1. The scheme of the dielectric heating of a NLC cell. Schadt's model corresponds to the case $\Delta T_g(t)=0$.

sume that the heat flux Q_{out} at the interface between the bounding plate and the surrounding medium obeys Newton's cooling law, i.e., $Q_{out}=k[T(\tilde{z}=L,t)-T_0]$, where $T(\tilde{z}=L,t)$ is the temperature of the outer boundary of the plates, T_0 is the temperature of the surrounding medium at infinity, and k is the heat transfer coefficient of the surrounding medium. The boundary conditions are then written as

$$\frac{\partial T(\tilde{z}=0,t)}{\partial \tilde{z}}=-\frac{Pd}{2G}, \quad \frac{\partial T(\tilde{z}=L,t)}{\partial \tilde{z}}=-\frac{k}{G}[T(\tilde{z}=L,t)-T_0],$$

$$(4)$$

where $T(\tilde{z}=0,t)$ is the temperature of the NLC-bounding plate interface. The solution for the temperature field in the glass plate $T(\tilde{z},t)$ of Eq. (3), supplemented with the boundary conditions in Eq. (4) and the initial condition $T(\tilde{z},t=0)=T_0$, is

$$T(\tilde{z},t) = T_0 + \Delta\bar{T}_k\left[1 + \xi\left(-\frac{\tilde{z}}{L}+1\right)\right.$$
$$\left. - \sum_{n=1}^{\infty} a_n \cos q_n \frac{\tilde{z}}{L} \exp\left(-\frac{t}{\tau_n}\right)\right],$$

$$(5)$$

where

$$\Delta\bar{T}_k = \frac{(2\pi f\varepsilon_0\varepsilon_{zz}^i + \sigma_{zz})U^2}{4kd}$$

$$(6)$$

is some characteristic temperature drop; as we shall see later, $\Delta\bar{T}_k$ is the stationary value of the temperature difference between the bounding plate's external boundary $\tilde{z}=L$ and the point $\tilde{z}\rightarrow\infty$ in the surrounding medium. The constant $\xi =kL/G$ is called the Biot number,[13] $a_n =2\tan q_n/(\sin q_n \cos q_n+q_n)>0$ are the dimensionless coefficients with the eigenvalues q_n satisfying the equation $q_n \tan q_n=\xi$, and $\tau_n=c_p\rho L^2/Gq_n^2$ are the characteristic time constants determining the transition to the stationary regime. For the convenience of further analysis, we will consider the temperature change $\Delta T(t)$ of NLC measured as the difference between the temperature T_0 of the NLC bulk and the temperature at infinity $\tilde{z}\rightarrow\infty$ (which is also the initial temperature of the whole system),

$$\Delta T(t) = \Delta\bar{T}_k\left[1 + \xi - \sum_{n=1}^{\infty} a_n \exp\left(-\frac{t}{\tau_n}\right)\right],$$

$$(7)$$

as the sum of the following two contributions:

$$\Delta T(t) = \Delta T_k(t) + \Delta T_g(t),$$

$$(8)$$

where

$$\Delta T_k(t) = T(\tilde{z}=L,t) - T_0 = \Delta\bar{T}_k\left[1 - \sum_{n=1}^{\infty} a_n \cos q_n \exp\left(-\frac{t}{\tau_n}\right)\right]$$

$$(9)$$

is the difference between the temperature $T(\tilde{z}=L,t)$ of the bounding plate's external boundary and T_0, and $\Delta T_g(t) =T(\tilde{z}=0,t)-T(\tilde{z}=L,t)$ is the temperature difference across the bounding plate, Fig. 1. Note that the previous model[7] assumes $\Delta T_g(t)=0$.

As one can see from Eqs. (6)–(9), the stationary value $\Delta T_k(t\rightarrow\infty)$ is indeed equal to $\Delta\bar{T}_k$; besides, $\Delta T_g(t\rightarrow\infty) =\Delta\bar{T}_g=\xi\Delta\bar{T}_k$. Therefore, the temperature increase of the NLC slab, $\Delta\bar{T}=\Delta T(t\rightarrow\infty)$, can also be represented by the sum of two terms:

$$\Delta\bar{T} = \Delta\bar{T}_k + \Delta\bar{T}_g = \frac{(2\pi f\varepsilon_0\varepsilon_{zz}^i + \sigma_{zz})U^2}{4kd}(1+\xi).$$

$$(10)$$

The model above, Eq. (10), suggests that one can distinguish two regimes of electric heating. When $\xi\gg 1$, the temperature increase of the NLC is controlled mainly by the temperature gradient in the bounding (glass) plates. For $\xi\ll 1$, the dominating control parameter is the heat transfer coefficient k of the surrounding medium, $\Delta\bar{T}\approx\Delta\bar{T}_k$. Qualitatively, Schadt's model[7] corresponds to the limit of $\xi\ll 1$ and effectively neglects the temperature gradients in the bounding plates by setting $\Delta\bar{T}_g=0$. Note that in the limit $\xi\ll 1$, Schadt's model and our model predict the same *stationary* values of the temperature increase; however, the *dynamics* of the temperature increase in the regime $\xi\ll 1$ is different in these two models.

Equations (7)–(10) indicate that the NLC temperature change is influenced by many factors, including the LC's imaginary dielectric permittivity component ε_{zz}^i, electric con-
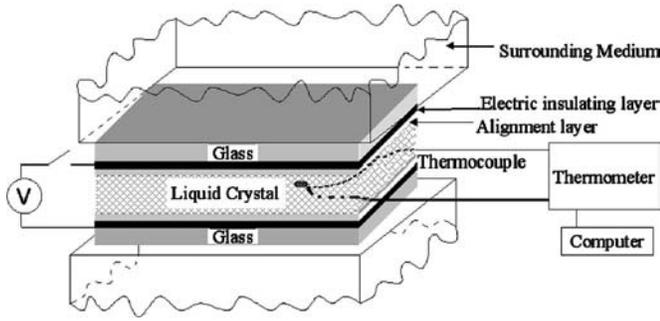
FIG. 2. Experimental setup to measure the temperature of the nematic cell driven by the electric field.

ductivity σ_{zz}, electric field (voltage U and frequency f), thermal properties of the surrounding medium (heat transfer coefficient k), and properties of the bounding plates (thermal conductivity G, heat capacity c_p, and thickness L).

In the experimental part, we will verify the predictions of the theory for different surrounding media and different electric fields. We demonstrate that the stationary temperature increase $\Delta \bar{T}$ scales as U^2; the implication of this result is that the temperature dependence of the material properties (neglected in the theory) does not play a significant role. The dynamics of temperature increase depends on the thermal properties of the surrounding medium and is well fitted by the theory above. In particular, for a given NLC cell in a given medium, the time needed to achieve $\Delta \bar{T}$ does not depend on the amplitude and frequency of the applied voltage (despite the fact that $\Delta \bar{T}$ itself does depend on both of them). The experiment also shows that $\Delta \bar{T}$ is a nonmonotonous function of the field frequency. This fact finds its explanation in the theoretical dependence $\Delta \bar{T} \propto f \varepsilon_{zz}^i + \sigma_{zz}/2\pi\varepsilon_0$; the nonmonotonous dependence occurs when the decrease of the imaginary part of the dielectric susceptibility with frequency is more significant than the increase of the frequency itself.

III. EXPERIMENTAL METHODS AND MATERIALS

Indium tin oxide (ITO) coated soda lime glass plates (Optera Colorado Inc.) of the thickness $L=1.1$ mm are used to make the LC cells. The glass parameters are as follows: $c_p=840$ J kg^{-1} K^{-1},[14] $\rho=2.44\times10^3$ kg m^{-3},[15,16]   and $G=0.94$ W m^{-1}K^{-1}.[16]

Temperature measurements. To measure the NLC temperature, we inserted a tiny (25 μm) Chromega-Constantan thermocouple into the liquid crystal bulk. To avoid an electric contact of the thermocouple and ITO, we spin coated a thin (1 μm) electric insulating layer (Nissan AT-720A) onto ITO. The layer is thin enough to cause no effect on the ac component of the field and the temperature gradients in the system. The reference end of the thermocouple is placed in the surrounding medium with temperature T_0 which was close to 23 °C. The measured NLC temperature data were transferred from the i-8 thermometer (Newport Electronics Inc.) to the computer through the RS-232 interface (Fig. 2).

The glass plates were additionally coated with the aligning layers of a rubbed polyimide (Dupont 2555) to set a uniform unidirectional orientation of the director in the plane of the substrates. The cell thickness was set at $d=40$ μm by Mylar stripes. The lateral size of the cells was 2×2 cm^2 with the head of the thermocouple placed in the center.

An outstanding question in temperature measurements is whether the probe can alter the very process of thermal dynamics. Despite the small size of the thermocouple head, it is still significant as compared to the cell gap. To verify that the thermocouple does not affect the thermal dynamics of the system, we compared the data obtained by this technique to the data obtained by a noncontact birefringence technique proposed by Wen and Wu,[9] see Appendix. Such a comparison was performed when the birefringence technique is applicable, i.e., when (1) the material has a negative dielectric anisotropy, (2) the cell yields a strict planar alignment (zero pretilt angle), and (3) the electric field causes no hydrodynamics. The two sets of data agree very well which verifies the validity of the thermocouple technique.

Materials. The cell was filled with a dual frequency nematic (DFN) mixture MLC2048 (EM industries, NY). The case of DFNs is of special interest in our studies. In these materials, the real part of the dielectric anisotropy $\Delta\varepsilon(f) = \varepsilon_{\parallel}^r(f) - \varepsilon_{\perp}^r(f)$ changes its sign from positive at $f<f_c$ to negative at $f>f_c$, where the crossover frequency usually corresponds to the region of dielectric relaxation of $\varepsilon_{\parallel}(f)$ with a characteristic time $\tau_{\parallel}$, $f_c \approx (2\pi\tau_{\parallel})^{-1}$, and to the maximum of the dielectric heating. Typically, f_c is low, in the range from 1 kHz to 1 MHz,[7,17,18] which is the range in which most electric driving schemes are operating. For MLC2048, $f_c=15$ kHz at 23 °C. The DFNs are usually formed by mixtures with molecules that have significant permanent dipole moments; therefore, the dielectric heating effects are well pronounced. Furthermore, the sign reversal of the dielectric anisotropy at f_c makes it possible to study the role of different components of the dielectric tensor on the dielectric heating phenomenon (when $f<f_c$, the director aligns parallel to the applied electric field and perpendicular to it when $f>f_c$). The dielectric heating in DFNs is also important because f_c and other material parameters of these materials are strongly temperature dependent.[7,8,17,18] Finally, it is important to bear in mind that many conventional NLCs are actually DFNs at sufficiently high frequencies. For example, in the most popular nematic material pentylcyanobiphenyl (5CB), $f_c \approx 20$ MHz,[19] while in heptylcyanobiphenyl (7CB), $f_c \approx 9$ MHz (Ref. 20) (both measured at room temperature).

We determined the dielectric and conductive properties of MLC2048 by using the capacitance method. We prepared planar and homeotropic MLC2048 cells with a thickness of about 15 μm. The director deviations from strictly planar and homeotropic orientation were less than 1° as determined by the magnetic null technique.[21] The cell under test was placed in an LTS-350 hot stage (Linkam) permitting temperature stabilization at (23 ± 0.1) °C. In order to determine the real (ε^r) and imaginary (ε^i) parts of the dielectric permittivity of MLC2048, we measured the amplitude and the phase of the complex impedance of the cell using the impedance/gain-phase analyzer SI-1260 (Schlumberger Inc.) in the frequency range from 1 kHz to 1 MHz, using a small voltage 0.5 V, which allowed us to avoid director reorientation. Figure 3 shows that the sign of the dielectric anisotropy
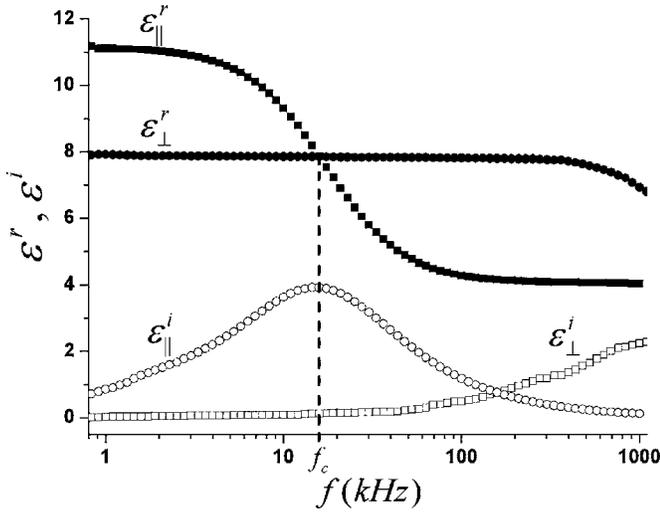
FIG. 3. The measured real components, $\varepsilon_\parallel^r$ and $\varepsilon_\perp^r$, and imaginary components, $\varepsilon_\parallel^i$ and $\varepsilon_\perp^i$, of the dielectric permittivity of MLC2048 in the frequency range of 1 kHz – 1 MHz at 23 °C. The error bars are smaller than the size of the data points.
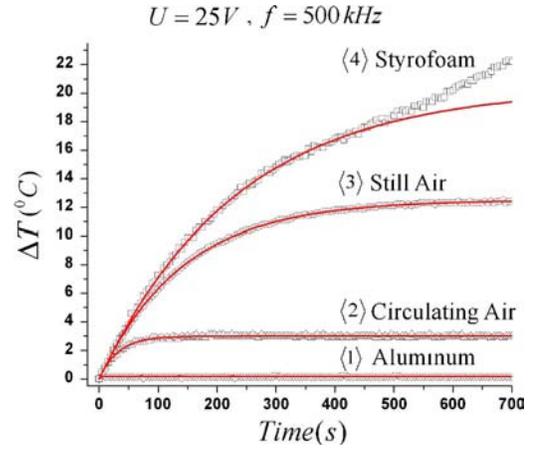

FIG. 4. (Color online) Temperature dynamics of a DFN MLC2048 cell surrounded by different media [(1)–(4)]. The initial temperature is 23 °C. The applied electric field has the voltage of 25 V and the frequency of 500 kHz. The accuracy of the temperature measurement is ±0.1 °C, with the error bars less than the size of the data points. The solid lines are theoretical fits of Eq. (11).

reverses from $\Delta\varepsilon > 0$ to $\Delta\varepsilon < 0$ with the crossover frequency $f_c = 15$ kHz, where f_c corresponds to the region of dielectric relaxation of $\varepsilon_\parallel(f)$. In a similar way, we estimated the ionic conductivity $\sigma \approx 10^{-9}$ Ω^{-1} m^{-1} using low frequencies $f \leqslant 100$ Hz; the anisotropy of conductivity turned out to be small, $\sigma_{zz} \approx \sigma_\parallel \approx \sigma_\perp \approx \sigma$.[10]

To examine how the heat transfer coefficient k of the surrounding media affects the electric heating-induced temperature rise of the NLC cell, we used the following line of the surrounding media, in which k is expected to decrease: (1) aluminum cooling devices, (2) circulating air, (3) still air, and (4) Styrofoam. In the experiment (1), we used the aluminum cooling devices P-2000 (Cyber Cooler, Inc.) composed of an aluminum radiator and a fan that are normally used as cooling fans for CPUs in computers. The NLC cell was sandwiched between the flat sides (lateral size of 2 × 2 cm^2) of the two devices with the fans switched on. To assure a good thermal contact between the glass and aluminum plates, we use a small amount of the thermal compound (Wakefield Engineering, Inc.) to fill the microgaps. In the experiment (2), the circulation of air was produced by the cooling fan P-2000 placed in such a way that the air flow was parallel to the surface of the NLC bounding plates. The distance between the cell edge and the fan was about 1 cm. In the experiment (3), the liquid crystal cell was hanged at two wires in the middle of the box with a size of 20 × 20 × 10 cm^3 made of a plastic mesh with the mesh density of 36/cm^2 and the square opening size of 1 mm. The function of the plastic mesh is to restrict the convection of the air flow. Note that most experiments with LC cells in academic laboratories and industrial devices fall between (1) and (3) situations. In case (4), the cell was sandwiched between two Styrofoam plates with a thickness of 5 cm each.

IV. EXPERIMENTAL RESULTS AND DISCUSSIONS

Figure 4 illustrates the temperature dynamics caused by the electric heating effect for the planar NLC cell placed in

four different surrounding media. The applied electric field ($U = 25$ V, $f = 500$ kHz) causes no director reorientation from the planar state. The temperature change is different in different media. First, the temperature change shows a tendency of saturation in media with good heat transfer (relatively high k). The temperature increase is small for the cooled aluminum surrounding and then increases in circulating and still air, which is a naturally expected result. For Styrofoam with poor heat transfer, the temperature increase is the largest and is not showing clear signs of saturation, at least within the time of experiment, Fig. 4.

Note that at the high frequencies used in our experiment, the electric heating effect is caused essentially by the dielectric mechanism. The Ohmic heating $P_\sigma = \sigma U^2/2d^2$ of the ionic current is negligibly small as compared to the dielectric heating because for the typical conductivity $\sigma \sim 10^{-9}$ Ω^{-1} m^{-1}, the ratio of the conductive heating to the dielectric heating, $P_\sigma/P \approx \sigma/\pi f \varepsilon_0 \varepsilon_{zz}^i$, is very small, less than 0.01 when $f > 3$ kHz. Therefore, in what follows, we will refer to the electric heating effect as to the dielectric heating effect.

Theoretically, Eq. (7), the NLC temperature increase $\Delta T(t)$ depends on series, $a_n \exp(-t/\tau_n)$. The first term $n = 1$ in this series is dominant, because of the two reasons. First, the characteristic times $\tau_n = c_p \rho L^2/G q_n^2$ with $n > 1$ are at least nine times smaller than τ_1 and shorter than 0.3 s. Really, by using $c_p = 840$ J kg^{-1} K^{-1},[14] $\rho = 2.44 \times 10^3$ kg m^{-3},[15,16] and $G = 0.94$ W m^{-1} K^{-1},[16] one finds $\tau_n = 2.6/q_n^2$ s; since $q_n > (n-1)\pi$, the largest relaxation time with $n > 1$ is thus $\tau_2 < 0.3$ s. Second, the first amplitude a_1 is at least six times larger than the sum of the amplitudes of all other terms. Equation (7) is then simplified to

$$\Delta T(t) = \Delta \bar{T}\left[1 - \exp\left(-\frac{t}{\tau_1}\right)\right],\tag{11}$$

where

$$\tau_1 = \frac{c_p \rho L^2}{G q_1^2}. \qquad (12)$$

Equation (11) describes the experimentally observed temperature dynamics for aluminum and air surrounding rather well, Fig. 4; it fits the experimental data with $\Delta \bar{T} = 0.2\,^\circ$C, $\tau_1 = 1.3$ s (1), $\Delta \bar{T} = 3.0\,^\circ$C, $\tau_1 = 32.2$ s (2), and $\Delta \bar{T} = 12.5\,^\circ$C, $\tau_1 = 141.8$ s (3). However, Eq. (11) does not describe the Styrofoam experiment (4). Figure 4 shows an unsuccessful attempt to fit the data with parameters $\Delta \bar{T} = 20.4\,^\circ$C, $\tau_1 = 233.3$ s, in Eq. (11); the fit is relatively good only at the early stages of heating. The departures are most naturally related to the fact that Newton's cooling law, used in the boundary condition in Eq. (4), is not justified. Newton's cooling law describes the convective heat transfer at the interface between a solid object and a flowing environment such as air or moving fluid. In fact, this flow keeps the temperature of the flowing medium at the interface constant, which is the case most closely matched in our experiments with the aluminum cooling devices and circulating air. For still air, Newton's cooling law is not expected to work as well, but the fit is still good. In contrast, poor heat transfer properties of Styrofoam lead to its gradual heating; as a result, Newton's cooling law is not applicable, as seen from the experimental data for Styrofoam surroundings.

The data collected in Fig. 4 allow us to determine the heat transfer coefficients from the fitted values of τ_1 and $\Delta \bar{T}$. We first determine $q_1 = L\sqrt{c_p \rho / G \tau_1}$ and then find k from the equation $q_1 \tan q_1 = kL/G$. For the aluminum cooling device, $k = 8267$ W m^{-2} K^{-1}; for circulating air, $k = 72$ W m^{-2} K^{-1}; and for still air, $k = 16$ W m^{-2} K^{-1}. The data for air are in the expected range of 10–100 W m^{-2} K^{-1}.[22] Moreover, by substituting the found values of k into Eq. (10) and using the experimentally measured $\Delta \bar{T}$, we find that the quantity $\varepsilon_{zz}^i = 1.8$ is the same for all three experiments with different media [(1)–(3)], as it should be, since ε_{zz}^i is the NLC material parameter (the imaginary part of the dielectric tensor component). The same value of ε_{zz}^i was measured independently by using the impedance analyzer SI-1260 (Schlumberger Inc.), Fig. 3, which testifies that the theoretical model describes the experimental data rather well.

The stationary temperature increase $\Delta \bar{T}$ is directly influenced by the heat generation rate determined by the electric voltage U and frequency f; according to Eq. (10), $\Delta \bar{T} = (1 + \xi)\Delta \bar{T}_k \propto f \varepsilon_{zz}^i U^2$. The dependence $\Delta \bar{T} \propto U^2$ is clearly confirmed in the experiments for aluminum and air surroundings, Fig. 5. Equation (10) matches the experimental data in Fig. 5 very well when one uses the independently measured $\varepsilon_{zz}^i = 1.8$ and the values of k found from the data in Fig. 4 for aluminum and circulating air. Note that Fig. 5 demonstrates that within the range of temperature increases studied in this work, the possible temperature dependencies of the material parameters such as ε_{zz}^i and k do not change the predicted linear dependence $\Delta \bar{T} \propto U^2$.

Equations (11) and (12) indicate that for a given NLC cell in a given surrounding medium the time τ_1 associated with the transition to the stationary state $\Delta \bar{T}$ does not depend
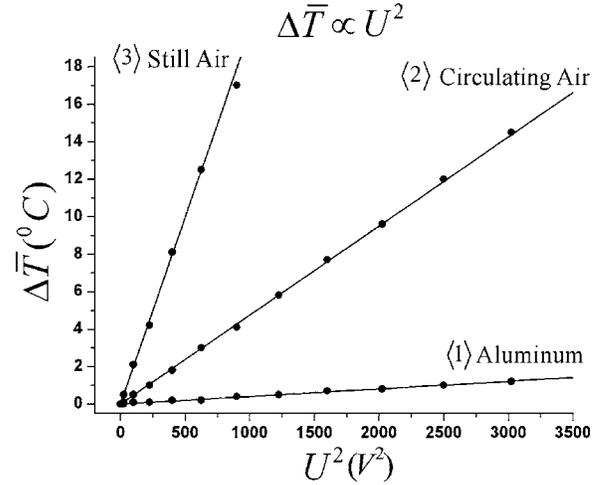

FIG. 5. Voltage dependence of the stationary temperature increase $\Delta \bar{T}$ for aluminum and air surroundings, measured at a constant $f = 500$ kHz. The initial temperature $T_0 = 23\,^\circ$C. The solid lines correspond to Eq. (10) with independently determined $\varepsilon_{zz}^i = \varepsilon_\perp^i = 1.8$ and $k = 8267$ W m^{-2} K^{-1} (1), $k = 72$ W m^{-2} K^{-1} (2), and $k = 16$ W m^{-2} K^{-1} (3). The accuracy of the temperature measurement is $\pm 0.1\,^\circ$C, with the error bars less than the size of the data points.

on the amplitude and frequency of the applied voltage (despite the fact that itself does depend on both of them). Figure 6 demonstrates that the dynamics of the temperature increase for the same system driven in different regimes with different voltages and frequencies can indeed be described with a single parameter τ_1. Interestingly, Fig. 6(a) shows also that the driving voltage of 45 V at $f = 0.8$ MHz produces a stronger dielectric heating effect than a higher voltage of 50 V at $f = 0.5$ MHz. The effect is related to the fact that the frequency of 0.8 MHz is closer to the frequency $f \approx 2$ MHz at which the imaginary part $\varepsilon_\perp^i$ for the studied DFN reaches a maximum.

Our model above indicates that the dielectric heating effect is strongly frequency dependent. There are different ways the frequency influences the temperature changes.

The first mechanism is through the direct dependency $\Delta \bar{T} \propto f$, see Eq. (10), which is predominant when the director is not experiencing reorientation in the field and when the frequency is far from the regions of dielectric relaxation. Furthermore, $\Delta \bar{T} \propto \varepsilon_{zz}^i$ and the temperature changes can be caused by the frequency dependencies of the LC dielectric properties, which give rise to mechanisms 2 and 3. The real components of the LC dielectric tensor are frequency dependent and changing the frequency of the applied field can change the director orientation θ, so that the effective imaginary dielectric permittivity $\varepsilon_{zz}^i = \varepsilon_\perp^i \sin^2 \theta + \varepsilon_\parallel^i \cos^2 \theta$ changes; we will refer to this effect as mechanism 2. Finally, the most interesting thing is that the temperature changes might reflect the nonmonotonous frequency dependencies of the imaginary parts $\varepsilon_\parallel^i$ and $\varepsilon_\perp^i$ of the parallel and perpendicular components of the dielectric tensor, i.e., through distinct mechanism 3.

The three mechanisms outlined above suggest that the total frequency dependency of the temperature increase, $\Delta \bar{T}$
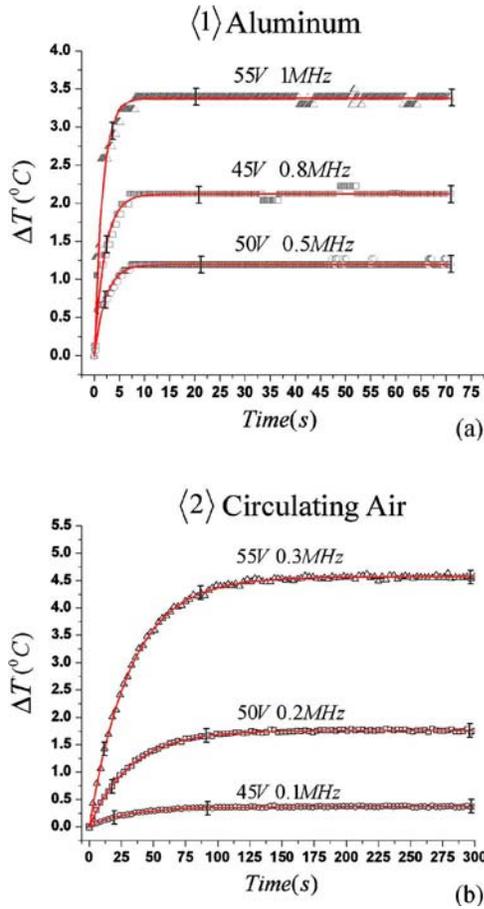
FIG. 6. (Color online) Temperature changes of the MLC2048 cells surrounded by the aluminum cooling device (a) and by circulating air (b), caused by different electric fields. The solid lines correspond to Eq. (11) with $\tau_1 = 1.5 \pm 0.2$ s (a) and $\tau_1 = 32.2 \pm 0.3$ s (b); $\Delta \bar{T}$ is determined experimentally. The accuracy of the temperature measurement is $\pm 0.1\,^\circ$C, and the corresponding error bars are demonstrated.
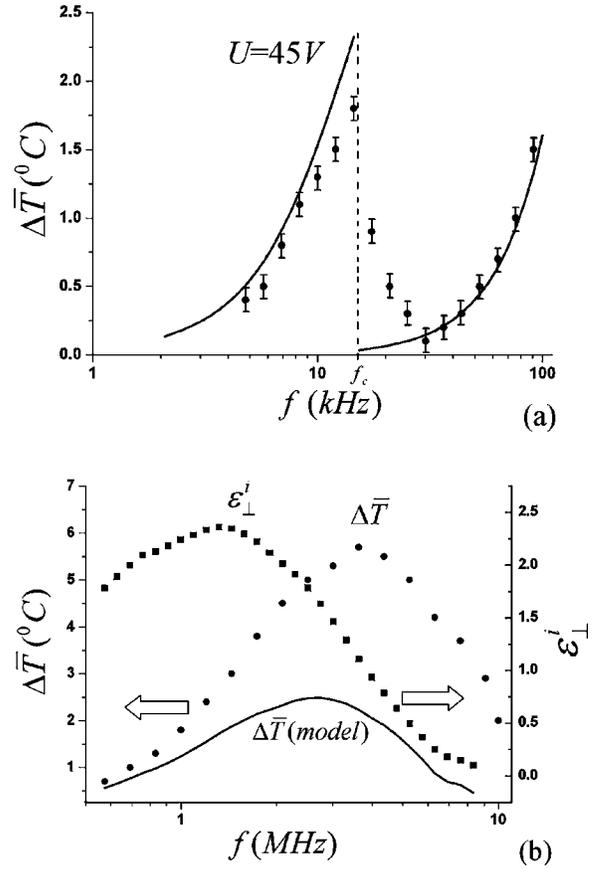

FIG. 7. (a) The stationary values of the temperature change $\Delta\bar{T}$ of the planar MLC2048 cell surrounded by medium (3) (still air) vs the applied frequency f, when f is in the range of the relaxation of $\varepsilon_\parallel$, 1–100 kHz. The solid line is the theoretical result calculated using Eq. (10) with most of the parameters measured directly (f, U, L, d, $\varepsilon_\parallel^i$, and $\varepsilon_\perp^i$); one parameter (G) was taken from Ref. 16 and one (k) was determined from the data shown in Fig. 4. The accuracy of the temperature measurement is $\pm 0.1\,^\circ$C, and the corresponding error bars are demonstrated. (b) Frequency dependence of the stationary values of the temperature change $\Delta\bar{T}$ of the planar MLC2048 cell surrounded by medium (3) (still air) and imaginary permittivity component $\varepsilon_\perp^i$ in the high-frequency range of 0.5–10 MHz. The solid line is calculated from Eq. (10) with no fitting parameters: the values of f, U, L, d, and $\varepsilon_\perp^i$ were measured directly; G was taken from Ref. 16 and k was determined from the data shown in Fig. 4.

$\propto f\varepsilon_{zz}^i(f)$, might be nonmonotonous, as $\varepsilon_{zz}^i(f)$ might be a decreasing function of f when f increases above the frequencies of the characteristic maxima for $\varepsilon_\parallel^i$, $\varepsilon_\perp^i$.

To verify experimentally the theoretical predictions, we used the still air surrounding (the temperature changes in circulating air and with aluminum cooling devices were too insignificant) for the LC cells. The temperature changes $\Delta\bar{T}$ at each frequency and voltage were determined as the stationary values, Fig. 7.

Figure 7 illustrates the three mechanisms above. Figure 7(a) shows the interplay of mechanisms 1 and 2. The cell with the original planar director orientation was driven by a high voltage of 45 V at different frequencies. At low frequencies, $f < f_c$, the director deviates from the initial planar orientation with $\theta = \pi/2$. As f increases, so does the temperature change $\Delta\bar{T}$, in accordance with mechanism 1, $\Delta\bar{T} \propto f$. However, the positive slope of $\Delta\bar{T}(f)$ changes to a negative one near $f \approx f_c$. This reverse in the slope in Fig. 7(a) can be associated with mechanism 2, i.e., with the director reorientation from the "vertical" state at low frequencies where $\Delta\varepsilon > 0$ to the "horizontal" (planar) state at $f > f_c$, where $\Delta\varepsilon < 0$, Fig. 3. Such a reorientation mitigates dielectric heating near $f \approx f_c$, as in this region, $\varepsilon_\perp^i < \varepsilon_\parallel^i$. Thus the dependency

$\Delta\bar{T}(f)$ in Fig. 7(a) results from the combination of mechanisms 1 and 2; note that this effect of the two competing mechanisms, 1 and 2, has been already observed and explained by Schadt.[7]

Figure 7(b) illustrates what might be a new type of $\Delta\bar{T}(f)$ dependence that is caused by the balance of mechanisms 1 and 3. By using the same planar cell as in the case shown in Fig. 7(a), we measured the temperature increase in the high-frequency regime above 0.5 MHz, Fig. 7(b). The applied voltage was small (5 V) The stability of the texture and the absence of director reorientation were verified under the microscope. We found that $\Delta\bar{T}(f)$ is nonmonotonous with a local maximum near $f = 4$ MHz. The most plausible reason of this nonmonotonous behavior appears to be the dielectric relaxation of $\varepsilon_\perp(f)$ manifested by a maximum of $\varepsilon_\perp^i$ at 1.8 MHz (mechanism 3), shown in Fig. 7(b). The fact that the maximum of $\Delta\bar{T}(f)$ is located at a higher f than the

maximum of $\varepsilon_\perp^i$ corresponds to the contribution of mechanism 1 to the total value of $\Delta\bar{T}(f)$. Figure 7(b) shows that the nonmonotonous behavior of $\Delta\bar{T}(f)$ is qualitatively reproduced by the model curve calculated using Eq. (10) with no fitting parameters. The quantitative difference between the experiment and theoretical prediction of Eq. (10) can be attributed to the following two reasons. First, the measurements of dielectric properties using the impedance/gainphase analyzer SI-1260 are not reliable at $f > 1$ MHz. Second, at the megahertz frequencies, the voltage acting at the liquid crystal layer is reduced as compared to the voltage applied to the entire cell by about 20%. However, this second factor should not cause the nonmonotonous behavior of $\Delta\bar{T}(f)$ by itself, as the quantity that matters is the product fU^2 that increases with f. Further experiments are needed to verify mechanism 3 quantitatively by accurately measuring the frequency dependence of $\varepsilon_\perp^i$.

V. CONCLUSIONS

We performed a systematic theoretical and experimental study of the electric heating effects in the nematic liquid crystals in an external ac electric field. A multilayer heat conduction model has been developed to understand how the temperature of a nematic cell confined between two plates and placed in a surrounding medium with certain thermal conductivity properties changes because of the electric heating effect. We derive the expressions describing the dynamics of temperature changes and the value of the stationary temperature increase. The temperature dynamics towards the stationary value follows the exponential law with the characteristic time τ_1 that depends on the bounding plates (their thickness L, heat capacity c_p, and thermal conductivity G) and on the heat transfer coefficient k of the surrounding medium. The stationary value of the temperature increase is a strong function of the applied voltage and nematic layer thickness, $\Delta\bar{T} \propto U^2/d$, the properties of the surrounding plates and medium, $\Delta\bar{T} \propto (1/k+L/G)$, and the field frequency, dielectric and conductive properties of the liquid crystal itself, $\Delta\bar{T} \propto f\varepsilon_0\varepsilon_{zz}^i + \sigma_{zz}/2\pi$. The conductivity contribution in our experiments becomes negligibly small at $f > 1$ kHz. Note that some of the parameters above, such as ε_{zz}^i, are itself temperature dependent. These dependencies do not change Eq. (10) for the stationary values of the temperature increase, but can somewhat modify Eq. (7) for the temperature dynamics. In most cases, however, these corrections are small, as demonstrated by the fact that the experimental dynamics is well described by Eq. (7).

The model assumes that the heat flux at the bounding plate-surrounding medium interface obeys Newton's cooling law, which is a good approximation for all practical media with a normal heat transfer; as shown in the experiment, the assumption might be violated only in media with an extremely poor heat transfer such as Styrofoam.

In the experimental part, we directly measured the temperature variations of the nematic material by a tiny thermocouple. We used the dual frequency nematic material as it allowed us to test the regions of the dielectric relaxation which are located at relatively low frequencies (tens of kilohertz). At the very same time, the frequency region of a few kilohertz and above corresponds to the situation when the electric heating caused by ionic currents is much smaller than the heating caused by dielectric relaxation. We used different surrounding media, from extremely good heat conductors such as aluminum cooling device to extremely poor conductor, Styrofoam; these two provide two limiting cases as compared to typical conditions of nematic cell exploitation in a laboratory or in commercial devices. The experiments with the good heat conductors confirmed that the NLC temperature changes are smaller in the media with a larger heat transfer coefficient k. The experiments confirm the theoretical predictions, namely, $\Delta\bar{T} \propto U^2/d$, $\Delta\bar{T} \propto (1/k+L/G)$, and $\Delta\bar{T} \propto f\varepsilon_{zz}^i$. The latter dependence is controlled by three different mechanisms and might be nonmonotonous. The nonmonotonous character of $\Delta\bar{T} \propto f\varepsilon_{zz}^i$ is associated with the director reorientation and with the existence of maxima in the frequency dependence of the imaginary parts of the dielectric permittivity $\varepsilon_\parallel^i$ and $\varepsilon_\perp^i$.

APPENDIX

To check whether the thermocouple affects the thermal behavior of the NLC cell or not, we compare the temperature data read from thermocouple and the temperature data obtained from the noncontact birefringence technique proposed by Wen and Wu.[9] The working principle of the birefringence method is described briefly as follows. As we know, the light transmission intensity of a nematic cell with uniform alignment placed between two crossed polarizers can be written as
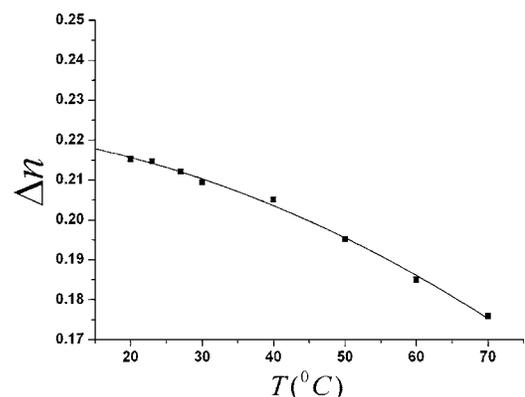

FIG. 8. Temperature dependence of birefringence Δn for MLC2048. The squares are the measured values, and the solid line is the polynomial fitting line, $\Delta n = \Delta n_0 + a(T-20) + b(T-20)^2$, where $\Delta n_0 = 0.216$, $a = -0.0047$, and $b = -6.8054 \times 10^{-6}$. The accuracy of the birefringence measurement is ± 0.001.
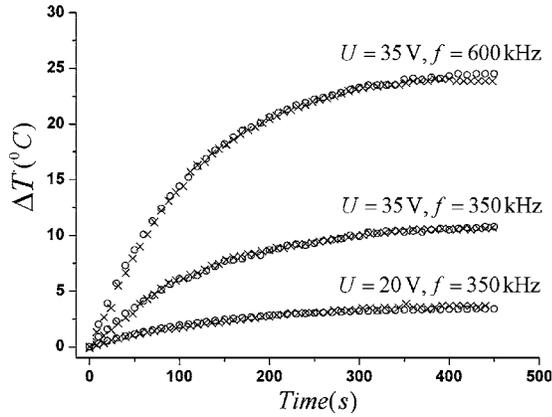
FIG. 9. The LC temperature change $\Delta T(t)$ measured by two methods. The circles are the temperature data read from the thermocouple, and the cross symbols are from the noncontact birefringence method. The accuracy of the direct temperature measurement using the thermocouple is ±0.1 °C, while the birefringence approach gives ±0.5 °C.

$$I = I_0 \sin^2 2\beta \sin^2 \Delta\varphi$$
$$= I_0 \sin^2 2\beta \sin^2 \left[\frac{\pi d}{\lambda} \left(\frac{n_o n_e}{\sqrt{n_e^2 \cos^2 \theta + n_o^2 \sin^2 \theta}} - n_o \right) \right],$$
$$\tag{A1}$$

where θ is the angle between **n** and the normal $\hat{\mathbf{z}}$ of the bounding plates, β is the angle between the projection of the director **n** in the azimuthal plane and polarization of the incident light, λ is the light wavelength, and n_e and n_o are the extraordinary and ordinary refractive indices, respectively. If the cell keeps the strict planar alignment during the whole period, $\theta = \pi/2$, one can obtain how the birefringence $\Delta n = n_e - n_o$ changes with time by recording the transmitted light intensity $I(t)$, Eq. (A2),

$$\Delta n(t) = \frac{\lambda}{\pi d} \{ k\pi \pm \arcsin[\sqrt{I(t)/I_0 \sin^2 2\beta}] \}. \tag{A2}$$

The temperature $T(t)$ at the moment t therefore can be derived once Δn as a function of the temperature T is identified. We use Abbe refractometer to measure the birefringence Δn of MLC2048 at a broadband range of temperatures (20–70 °C) and polynomially fit Δn as a function of T, Fig. 8.

To trace the birefringence dynamics $\Delta n(t)$, we measured the transmission light intensity of the 40 μm planar MLC2048 cell. The cell is thermally stabilized at (23±0.1) °C and placed between two crossed polarizers in such a way that the director projection onto the glass plates makes an angle 45° with the polarization axis, i.e., $\beta = 45°$. The cell is driven by the harmonic electric fields produced by the DS345 wave form generator (Stanford Research System).

Different electric fields are applied to the cell and the transmission light intensity change $I(t)$ is recorded and analyzed. The corresponding temperature $T(t)$ is derived by using Eq. (A2) and $\Delta n(T)$ which is obtained by the fittings in Fig. 8. Independently, we measured the LC temperature through the thermocouple, Fig. 9. The comparison of both data sets in Fig. 9 confirms that the finite thermocouple does not affect the thermal behavior of the NLC cell under test.

[1] J. D. Jackson, *Classical Electrodynamics* (Wiley, New York, 1962).
[2] W. Haase and S. Wrobel, *Relaxation Phenomenon* (Springer, New York, 2003).
[3] C. J. F. Bottcher and P. Bordewijk, *Theory of Electric Polarization* (Elsevier, New York, 1978), Vol. 2.
[4] W. H. de Jeu, C. J. Gerritsma, P. van Zanten, and W. J. A. Goossens, Phys. Lett. **39**, 355 (1972).
[5] H. A. Haus and J. R. Melcher, *Electromagnetic Fields and Energy* (Prentice-Hall, Englewood Cliffs, NJ, 1989).
[6] Y. Yin, S. V. Shiyanovskii, A. B. Golovin, and O. D. Lavrentovich, Phys. Rev. Lett. **95**, 087801 (2005).
[7] M. Schadt, Mol. Cryst. Liq. Cryst. **66**, 319 (1981).
[8] Y. Yin, M. Gu, A. B. Golovin, S. V. Shiyanovskii, and O. D. Lavrentovich, Mol. Cryst. Liq. Cryst. **421**, 133 (2004).
[9] C. H. Wen and S. T. Wu, Appl. Phys. Lett. **86**, 231104 (2005).
[10] L. M. Blinov and V. G. Chigrinov, *Electrooptical Effects in Liquid Crystal Materials* (Springer, New York, 1994).
[11] J. Fourier, *The Analytical Theory of Heat* (Dover, New York, 1955).
[12] G. Ahlers, D. S. Cannell, L. I. Berge, and S. Sakurai, Phys. Rev. E **49**, 545 (1994).
[13] A. V. Luikov, *Analytical Heat Diffusion Theory* (Academic, New York, 1968).
[14] T. Muneer, J. Kubie, and T. Grassie, *Heat Transfer: A Problem Solving Approach* (Taylor & Francis, New York, 2003).
[15] K. K. Chawla, *Composite Materials*, 2nd ed. (Krishan Kumar, Norwell, MA, 2003).
[16] http://www.valleydesign.com/sodalime.htm
[17] X. Ming and D. Yang, Appl. Phys. Lett. **70**, 720 (1997).
[18] M. Schadt, Mol. Cryst. Liq. Cryst. **89**, 77 (1982).
[19] B. A. Belyaev, N. A. Drokin, V. F. Shabanov, and V. A. Baranova, Phys. Solid State **46**, 574 (2003).
[20] T. K. Bose, B. Campbell, S. Yagihara, and J. Thoen, Phys. Rev. A **36**, 5767 (1987).
[21] T. J. Scheffer and J. Nehring, J. Appl. Phys. **48**, 1783 (1977).
[22] A. Bejan, *Heat Transfer* (Wiley, New York, 1993).